`Covalent' effects in `ionic' liquids

2000 J. Phys.: Condens. Matter 12 A95

(http://iopscience.iop.org/0953-8984/12/8A/310)

J. Phys.: Condens. Matter **12** (2000) A95–A108. Printed in the UK PII: S0953-8984(00)09520-5

'Covalent' effects in 'ionic' liquids

Paul A Madden and Mark Wilson

Physical and Theoretical Chemistry Laboratory, Oxford University, South Parks Road, Oxford OX1 3QZ, UK

Received 15 November 1999

Abstract. Many binary systems (and their mixtures) which might be expected to be 'ionic', from electronegativity considerations, are found to exhibit pronounced 'covalent effects' in their condensed-phase structure and dynamical properties. Recent work, involving both electronic structure calculations and computer simulation, has suggested that the interactions arise and are describable within the ionic model—provided that many-body effects, whose origin is the change in an ion's properties caused by interaction with its environment, are included. In systems where they are substantial, the many-body effects promote remarkably rich changes in the intermediate-range structure of an ionic liquid. $AlCl_3$ becomes molecular, $BeCl_2$ a 'living polymer' of extended chains, and the distinctive intermediate-range order (IRO) of the three-dimensional-network, glass-forming systems $ZnCl_2$, BeF_2 and SiO_2 is reproduced. The structural changes have considerable dynamical consequences: for $ZnCl_2$ the slow structural relaxation, leading to the glass transition, may be traced back to the relaxation of the IRO. On shorter timescales (higher frequency) these liquids exhibit spectroscopic bands usually assigned to quasi-molecular units. The formation and dissociation of these units is crucial in ionic conduction, and other transport properties.

(Some figures in this article appear in black and white in the printed version.)

1. Introduction

From the current dominance of 'complex fluids', composed of polymers, surfactants and colloids, in the literature of liquid-state physics, it might be supposed that atomistic fluids present no significant challenges for understanding or are already thoroughly characterized. Here we will focus on binary liquids composed of elements with significantly different electronegativities, and hope to show that they present exciting conceptual issues, whose consequences have been barely addressed. (We will only deal with stoichiometric mixtures, where the composition matches the valency of the element concerned—as in $MgCl_2$, Al_2O_3 etc—more general combinations present even greater challenges.) At a practical level, the use of such liquids has been proposed in numerous *new* technologies, such as nuclear and other waste reprocessing and containment. These technologies, as well as the optimization of older ones, like aluminium extraction, pose questions about the properties of these fluids to which the field is currently unable to provide answers. Furthermore, new types of experimental information, particularly relevant to these fluids, is coming through the introduction of advanced radiation facilities in Europe, the US and Japan. Reliable structural information from EXAFS and from anomalous x-ray scattering, and dynamical information from inelastic x-ray measurements is now becoming available. The development of new containment techniques for corrosive liquids at high temperatures (and pressures) has opened up new classes of liquids for microscopic characterization for the first time, and also allowed such techniques as nmr and Raman spectroscopy to be applied systematically.

0953-8984/00/SA0095+14$30.00

The fascination of these liquids lies in the wide range of local structural arrangements which can arise, and in connecting this structure to thermodynamic (phase equilibria) and transport properties. The range of structures is much broader than in van der Waals liquids, where packing considerations dominate, and, as we shall see, intermediate as well as purely nearest-neighbour length scales become important. The richness of structures is also the feature which has inhibited systematic approaches to the subject, as they are conventionally attributed to 'covalent' interactions which might be different in each material studied and therefore preclude a general description. In fact, as we hope to illustrate below, these structures arise from well-defined and general interactions which follow from basic physical principles, and which are straightforwardly represented. This standpoint is one which has been argued by Tosi, in particular [1, 2].

2. An extended ionic interaction model

It is well known that the domain of applicability of the simplest ionic model, as embodied in Born–Mayer-type pair potentials, is severely restricted:

$$U_{BM} = \sum_i \sum_{j(\to i)} A \exp[-(r_{ij} - \sigma_i - \sigma_j)/(\rho_i + \rho_j)] + Q_i Q_j / r_{ij}. \tag{2.1}$$

Here r_{ij} is the separation between i and j and Q_I the charge. We think of the exponential repulsion as arising from the overlap of cation and anion charge densities, of which σ is a characteristic radius and ρ the shape. With suitably chosen values for σ and ρ, such a potential will reproduce quite accurately the liquid and solid structures of NaCl [3]. However, even for $MgCl_2$ or $ZnCl_2$, where the large electronegativity differences between the elements involved would be expected to make an ionic picture of electronic structure equally valid, the BM potential fails *qualitatively* to reproduce the structures observed. This failure is illustrated in figure 1, where the experimental partial radial distribution functions (prdfs) [4, 5] of $ZnCl_2$ are reproduced and compared with the predictions of a BM potential (which reproduces the Zn–Cl separation and coordination number). In the experimental data, the first peaks in the Cl–Cl and Zn–Zn prdfs coincide, indicating that the nearest-neighbour Cl–Cl and Zn–Zn distances are equal. But this disagrees with the simple ionic picture where the doubly charged Zn^{2+} ions repel each other more strongly than the Cl^- ions, leading to a larger Zn–Zn separation, as shown in the data for the BM potential.

It cannot be concluded that this is a failure of an ionic model of the interactions *per se*—only that it is a failure of its simplest manifestation in the BM potential, where the electron densities of the ions are implicitly regarded as rigid. A more general ionic model would retain the idea that ions are electronically closed-shell species with formal (valence) charges so that the only *possible* [6] interactions between them are a repulsion, whose origin is the Pauli exclusion principle, at such short range that the electron densities overlap, and dispersion, polarization and Coulombic interaction of the charges at longer range. However, it is not sufficient to think of a condensed phase of ions as a collection of well-defined, gas-phase species. A van der Waals material, such as a rare gas or molecular solid, can be quite accurately modelled this way, but in ionic materials the ions themselves are profoundly influenced by their environment. The oxide ion, for example, is unstable in the gas phase but commonly occurs in condensed matter.

More quantitative manifestations of these environmental effects on the electron density are illustrated in figures 2 and 3. In figure 2 the dependence of the polarizability of an F^- ion in a series of cubic crystals is shown as a function of the lattice parameter [7], R. At large R ($\to\infty$) the electron density relaxes back to that of the free ion and the polarizability

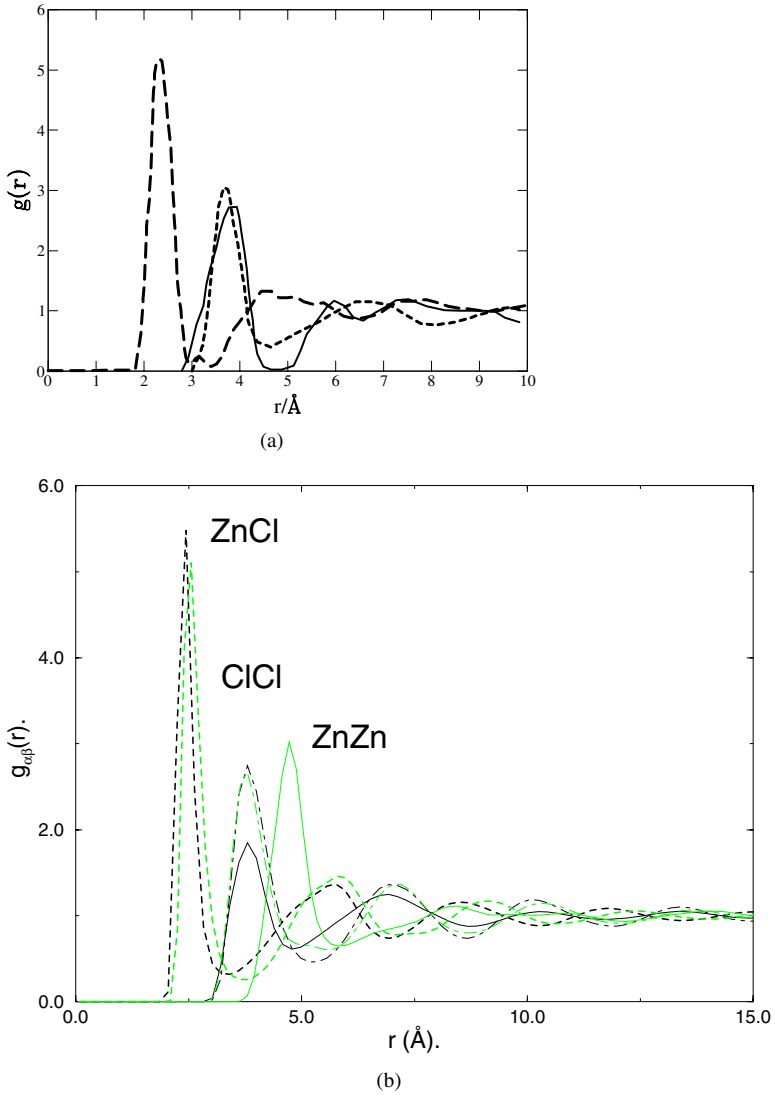

Figure 1. The experimental partial radial distribution functions for $ZnCl_2$ (a) [4] are compared with (b) prdf predicted with a simple pair potential (RIM)—light lines—and when the potential additionally includes polarization effects (PIM)—black lines. Interest centres on the relative positions of the first peaks in the Cl–Cl and Zn–Zn prdfs.

to the free-ion value of about 16.5 au, but as R is reduced to more typical condensed-phase separation, its value is much decreased. Since the polarizability is a measure of the spatial extent and distortability of the electron density, the figure illustrates just how compressed the condensed-phase ion is relative to its free counterpart. It indirectly shows that we must expect the size of an anion, which appears as a fixed parameter (σ) in the BM potential, to vary between different coordination environments [8, 9]. The figure also illustrates how systematic this R-dependence of the polarizability is in different materials; the relationship between the curves for the different alkali fluorides may be understood, quantitatively, through the differences in cationic radii.

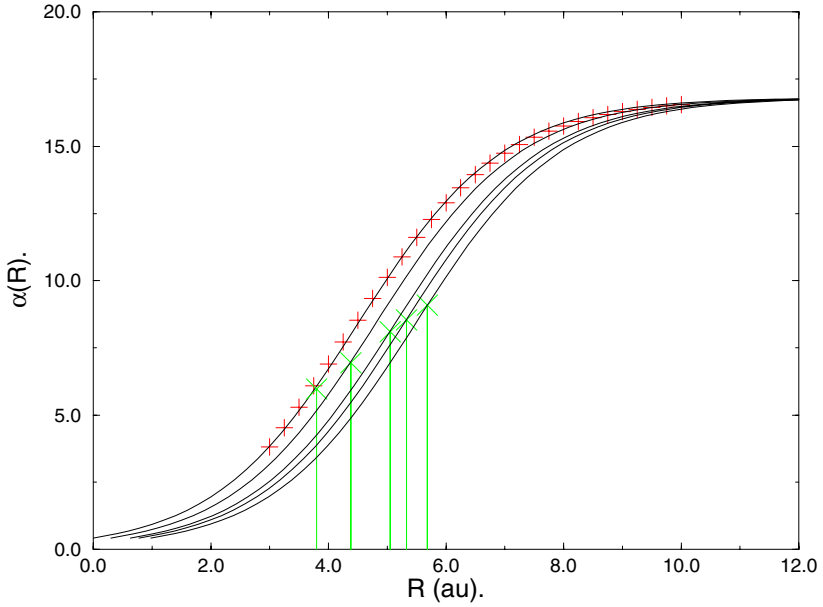

Figure 2. The polarizability (in atomic units) of an F^- ion in a series of alkali fluorides (from left to right, LiF, NaF, KF, RbF, CsF) is shown as a function of the lattice parameter R [7]. The equilibrium lattice parameter of each material is shown as a vertical line and cross.

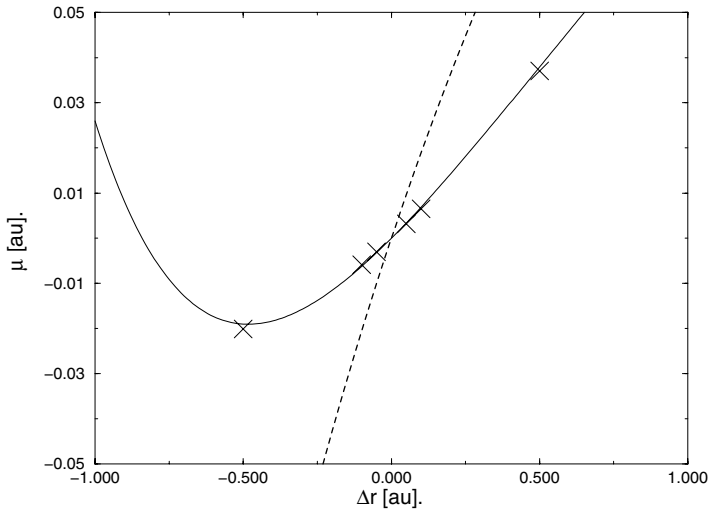

Figure 3. The induced dipole on an F^- ion in a cubic crystal which has been distorted by the radial displacement of a first-neighbour cation from its lattice position (crosses) [10] by Δr (in bohrs). The dashed-line shows the Coulombic (or asymptotic) dipole predicted from the electric field at the anion site, so the difference between the points and the solid line is attributable to the short-range effect.

In figure 3 one of the effects of lowering the symmetry of an anion's environment is shown. In these calculations [10], one of the cations in the first coordination shell around an anion in the cubic crystal has been displaced off its lattice site by the distance Δr and the resulting

induced dipole on the anion is shown. This displacement generates electric fields ($\boldsymbol{E}$), and field gradients ($\boldsymbol{E}'$) on the anion and these induce a dipole moment [11]

$$\mu_\alpha^{i,as} = \alpha_{\alpha\beta} E_\beta(\boldsymbol{r}^i) + \frac{1}{3} B_{\alpha\beta,\gamma\delta} E_\beta(\boldsymbol{r}^i) E'_{\gamma\delta}(\boldsymbol{r}^i) + \cdots \tag{2.2}$$

where α and B are polarizabilities. However, as the data show, this is not the only contribution to the dipole. Since the anion's electron density is already highly compressed by its coordination environment in the undistorted crystal, displacement (say outwards) of one of the first-shell cations allows the electron density to relax into the space created, and thereby creates a 'short-range' dipole which opposes and significantly cancels the electric field-induced one $\mu^{i,as}$.

Because of such effects, the interaction of one ion with another cannot be expressed without reference to the environment in which each ion is found. Consequently, an interaction potential expressed purely in terms of ionic positions must be expected to have an *explicit* many-body character—unlike the van der Waals case, where pair potentials (which may implicitly include the average effects of weak many-body interactions) are the norm. In a melt, the environment will change from one instant to the next.

The effects may be included in an 'extended' ionic interaction potential [12], in which instantaneous values of the ionic properties such as the dipole and the ion size appear as variables alongside the ionic positions. These additional variables characterize the instantaneous state of the electron density of each ion or, rather, those aspects of it which are needed to specify the interactions. The forms of these potentials may be uncovered from *ab initio* electronic structure calculations on idealized reference configurations, as illustrated above. The dynamics of the additional variables in a molecular dynamics simulation may be handled by borrowing ideas from the Car–Parrinello *ab initio* MD method. These technical matters have been described in a number of papers [9, 12]; here we will survey the consequences of the many-body effects for the structure and dynamics of a wide range of ionic systems. The subtext is that much 'covalent' behaviour is quantitatively explicable within the extended ionic interaction model.

3. Structural consequences of the many-body effects

The environment-induced changes in the ion size and shape are very important for oxides, and are crucial in explaining the preferred coordination in such systems. In halides, on which we will focus below, these effects are much less significant [13]; deficiencies of the pair potential representation of the short-range repulsion are not marked. Good progress can be made by supplementing the Born–Mayer potential described earlier with an account of the halide-ion polarization effects.

3.1. MX_2 systems

A snapshot of the structure in a $ZnCl_2$ melt [14], simulated with such a potential model is shown in figure 4. It can be seen that the local structure consists of a tetrahedral arrangement of Cl^- ions around each Zn^{2+}; this is an ion-size effect, contained within the pair potential, and is a property of the structures obtained when the polarization effects are included or omitted. The polarization effects influence the way these tetrahedral units are linked. The simple BM pair potential predicts linear Zn–Cl–Zn bridges, in order to minimize the cation–cation Coulomb repulsion. The polarizable model, on the other hand, gives a bent 'bond' with a bond angle of $\sim 110^\circ$. The fact that the Zn–Zn distance is shortened in this way brings the prdf for the polarizable model into agreement with experiment.

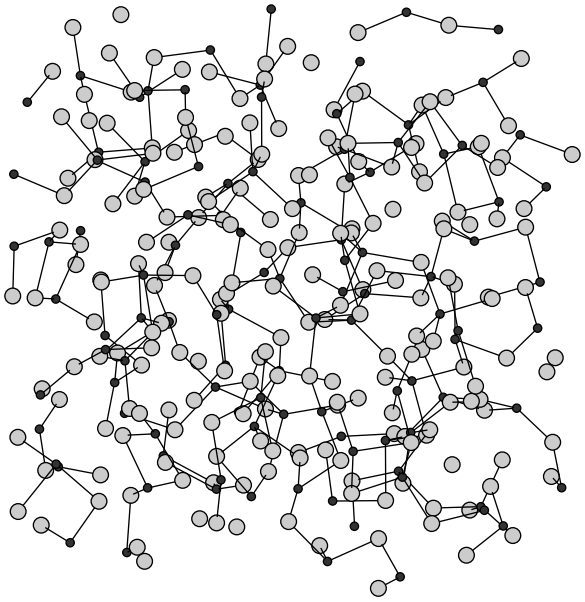

(a)

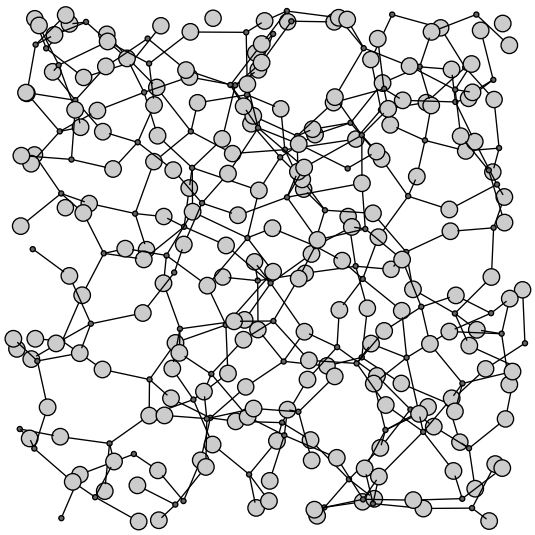

(b)

Figure 4. Snapshots of the ionic positions in simulations of (a) $ZnCl_2$, (b) BeF_2 [15] and (c) $BeCl_2$ melts with a polarizable-ion model. Cations are small and dark and the anions are larger and more lightly shaded. Note the predominant tetrahedral coordination, but the different *inter*-tetrahedral connections.

Figure 5 shows that polarization is the driving force for the occurrence of this non-trivial bond angle, a phenomenon often attributed to 'covalency'. If the bond were linear, the Cl^- would be symmetrically located between two cations and no induced dipole could result. If, on the other hand, the Cl^- is displaced off the line of centres of the cations, a dipole is induced, which serves to screen the cation repulsion and lowers the total energy. A more open structure,

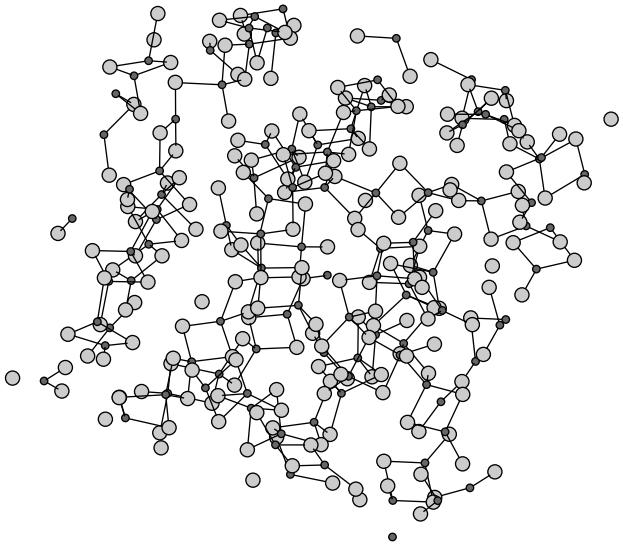

(c)

Figure 4. (Continued)

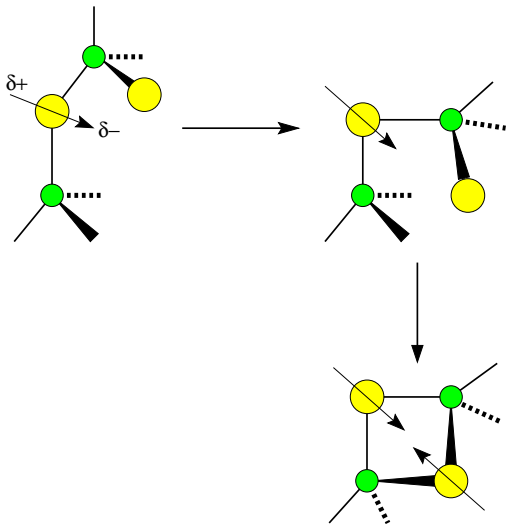

Figure 5. The figure illustrates the induced dipole as a driving force for bond bending and how, with decreasing cation size (increasing polarization effects), this eventually favours a polyhedral edge-sharing motif.

containing voids, results, so the price paid for the polarization energy is an increase in the Coulomb, or Madelung energy.

The specific consequences of the polarization effects depend on a subtle interplay between them, the straightforward Coulombic interactions between the ionic charges and excluded-volume effects, as determined by the ion-size ratio and stoichiometry. The polarization effects become more important for highly polarizable ions, and when the cation radius is significantly smaller than the anionic one. For larger cations, the simple ionic structures, with an anion interposed between the cations, emerge as most stable. At intermediate size, this bridge becomes bent, as illustrated above, resulting in corner-linked polyhedra. For very small cations and polarizable anions the bending is such as to give edge-linked polyhedra in which the induced

dipoles on *two* anions screen the cation–cation repulsion, as indicated in figure 5.

This sequence may be illustrated by contrasting $ZnCl_2$ with BeF_2 [15] (figure 4(b), where polarization effects are smaller due to the smaller F^- polarizability, and $BeCl_2$ [16] (c), where they are larger due to the smaller cation. In BeF_2, the greater bond angle results in an almost ideal network of corner-sharing tetrahedra. In $BeCl_2$, *edge*-linked tetrahedra form long chains which are terminated at occasional three-coordinated Be sites (the radius ratio for Be^{2+} to Cl^- puts it at the lower edge of stability for fourfold coordination). The result is a liquid of charge-neutral polymeric molecules, which break up and re-form in the melt, resulting in a 'living polymer'.

The consequences of these changes in the degree of bond bending caused by the polarization effects are much more profound than simple changes in the relative positions of peaks in prdfs. In the fully corner-connected tetrahedral network (like in BeF_2) each cation is pinned in place by four bonds to distinct neighbours and the network can only relax by some bond breaking. If there is some degree of edge sharing, the degree of connectivity of the network is reduced and some increase in its fluidity is to be expected. In the extreme case of $BeCl_2$ the 'network' is completely loose, since a given ion may be transported by a bodily translation of the polymeric molecule in which it is located. The relationship between the connectivity of the bonding network and its rigidity has been expressed by Phillips [18] and Thorpe [17], and the 'strength' of the fluid has been discussed in these terms by Angell [19]. From this discussion, we can see why BeF_2 should be a stronger fluid than $ZnCl_2$ and we would expect $BeCl_2$ to be a fragile polymer. Although it is possible to heuristically connect the fluidity to the structure and thereby to the underlying interactions in this way, it has not yet proven possible to show in detail how the mechanism of ionic motion depends on the structure.

3.1.1. Intermediate-range order. The changes in network structure (whilst preserving the local tetrahedral ordering of anions about cations) result in characteristic changes in diffraction patterns on *intermediate* length scales. In figure 6 we contrast the cation–cation (Zn–Zn) partial structure factor ($S_{++}(k)$) calculated in simulations of $ZnCl_2$ when the polarization effects are included (PIM) or excluded (RIM) with all other interactions left the same. The RIM structure factor is typical of a simple ionic liquid, with a strong principal peak at a wavevector (k) equal to roughly $2\pi/r_{++}$, where r_{++} is the cation–cation distance of closest approach, i.e. the position of the first peak in g_{++} in figure 1. There is no significant structure at lower k, indicating that the liquid structure on length scales longer than r_{++} is in some sense trivially determined by this distance too. On introducing the polarization effects, we see that this principal peak splits. The component which moves to higher k ($\sim$2.0 Å^{-1}) should be regarded as the new principal peak, as it is related to r_{++} in the polarizable fluid. It has gone to higher k than in the RIM model because this cation–cation separation has shortened, for the reasons discussed above. More dramatically, a new peak has appeared at lower k ($\sim$1.0 Å^{-1}). This is a 'prepeak' or 'first sharp diffraction peak' (FSDP) [20] and indicates that a new length scale has become important in determining the structure of the fluid. This PIM-predicted $S_{++}(k)$ agrees well with that observed experimentally [4].

Also shown in figure 6 is $S_{++}(k)$ for BeF_2 [15], where the network structure is less affected by polarization effects than in $ZnCl_2$ and will be closer to that predicted with the simple ionic RIM. Here we see that the FSDP is less pronounced than in the PIM $ZnCl_2$ and is best described as a shoulder on the principal peak.

The best way to describe the intermediate-range order, as manifested in the FSDP, has been much discussed [20]. As the relevant length scale is that of the *next*-nearest neighbour (and beyond) it has no clear signature in the corresponding rdf. Elliott [21] has suggested that it is useful to characterize the new length scale as an *inter-void* correlation length, and simulation

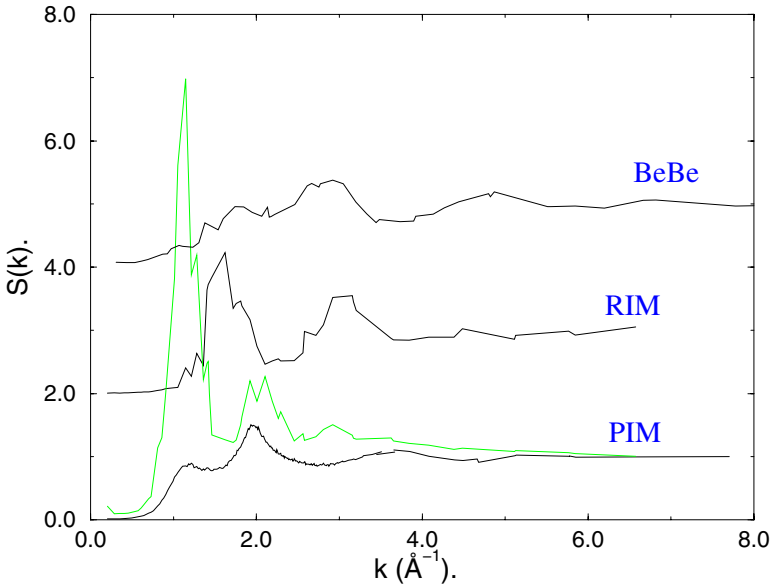

Figure 6. The cation–cation partial structure factors ($S_{++}(k)$) calculated for $ZnCl_2$ at the RIM (shifted by +2) and PIM levels are compared; note the appearance of an FSDP at $\sim$1 Å^{-1} in the PIM calculation. The FSDP position is seen to coincide with the principal peak of the void–void structure factor (light line). $S_{++}(k)$ for BeF_2 is also shown (shifted by +4), where the IRO dictates a different relationship between the FSDP and principal peak.

studies of several liquids [22] (including water) have shown the generality of this association. Examination of figure 4 shows why this is a helpful way of characterizing the shape of the network. As a result of the bond-bending effect, which pulls nearest-neighbouring pairs of Zn ions closer together than they would have preferred under simple Coulomb repulsion, the distribution of Zn ions has become more patchy and appreciable spaces (voids) have opened up. The network winds its way around these voids, and the inter-void separation becomes a measure of the associated length scale.

3.2. MX_3 systems

This polarizable-ion model of halide melts suggests that structural trends should depend on the cation radius in a group of systems with a common anion (and hence roughly constant anion size and polarizability). The trivalent metal halides provide an excellent opportunity to test this suggestion as trivalent cations appear in many parts of the periodic table and a wide range of radii is spanned (La^{3+}, U^{3+} $\sigma \sim 1.45$ Å, Al^{3+}, Fe^{3+} $\sigma \sim 0.6$ Å). Phenomenologically, there is a correspondingly wide range of liquid properties [1, 2, 5]—$LaCl_3$ is an ionic melt with a high freezing temperature, whereas $AlCl_3$ melts from an ionic crystal to a low-density *molecular* liquid. On the other hand, at intermediate size YCl_3 melts from the same crystal structure as $AlCl_3$ with a tiny volume change, which suggests almost continuous melting. Recent diffraction experiments [23, 24] have enormously increased the amount of structural information available on these systems and have enabled a systematic study of the structural trends.

The structures calculated with formal-charge, polarizable-ion potentials, which differ *only* through the cation radius, have been shown to reproduce extremely well [25] the experimental

structure factors across the series $LaCl_3 \rightarrow AlCl_3$. Examples at the extremes of the series ($LaCl_3$ [23] and $FeCl_3$ [24]) are shown in figure 7, where the agreement is typical of that achieved throughout. These extensive comparisons underpin the claim that the polarizable-ionic model reproduces the structures observed in a wide range of halide systems of MX_2 and MX_3 stoichiometry with minimal variation in potential parameters from one system to another and with physically meaningful values for polarizabilities, ion size etc. Unfortunately, space does not permit us to examine this claim more fully here.

4. Dynamical properties

That the wide range of structures exhibited by the MX_3 (and MX_2) systems may be traced back to a single generic ionic interaction potential eliminates the spectre of mysterious 'covalent' interactions and enables the investigation of how *dynamical* phenomena are governed by the properties of the local coordination polyhedra and their connections to begin. Foremost amongst these phenomena are the fluidity and conductivity, which must involve the breaking of the *inter*- and *intra*-polyhedral connections.

4.1. Structural relaxation in network liquids

In 'van der Waals' liquids, where the structure is dominated by packing effects, the structural relaxation which determines the viscosity is that of the cage around each particle. In the supercooled liquid the self-consistent relationship of the cage relaxation to the density fluctuations is embodied in the mode-coupling theory (MCT) [26], which predicts an ergodic–non-ergodic transition at an ideal glass transition temperature (T_c). Detailed MCT predictions appear to be well obeyed by many van der Waals systems (which are 'fragile' liquids [19]) as T approaches T_c from above. In network-forming (strong) liquids, like $ZnCl_2$ or SiO_2, simulation studies have shown that the long-time relaxation process is qualitatively consistent with MCT predictions. The shape of the time correlation functions (see figure 8) is as observed in fragile systems, exhibiting a plateau on intermediate (β) timescales; the long-time α-relaxation is stretched and obeys time–temperature superposition. However, the binary-liquid MCT equations appear not to describe the transition quantitatively for SiO_2 [27] and $ZnCl_2$. Note, however, that the molecular MCT appears to work extremely well for the related network liquid H_2O [28], which suggests that the failure for SiO_2 and $ZnCl_2$ is due to the breakdown of specific approximations, best suited to hard interactions, and not the general approach.

An examination of the relaxation of the density fluctuations in the liquid shows that the nature of the basic structural relaxation process may involve changes in the topology of the network, rather than the caging process which is captured so well in the MCT equations. Figure 8 shows the correlation functions of the Fourier components of the cation density in $ZnCl_2$ at wavevectors corresponding to the principal peak of the structure factor (see figure 6), to the FSDP position, and an intermediate wavevector. It is clear that the FSDP relaxation is substantially slower than that at the principal peak. Given that there is an appreciable weight in the static structure factor at the FSDP, it appears likely that relaxation at the FSDP will dominate the relaxation of the stress tensor in the fluid [29]. In water, the structure factors near to the FSDP in S_{OO} dominate the molecular MCT integrals and drive the glass transition [28], whereas in a van der Waals fluid, the dominant contributions are at the principal peak reflecting the dominant role of the relaxation of the first-neighbour cage in the structural arrest. As argued above, the FSDP reflects intermediate-range order in the liquid, which is non-trivial because of the network connectivity. Thus the relationship of density fluctuations to structural relaxation in the network fluid is analogous to that of a polymer melt. There the first peak in the structure

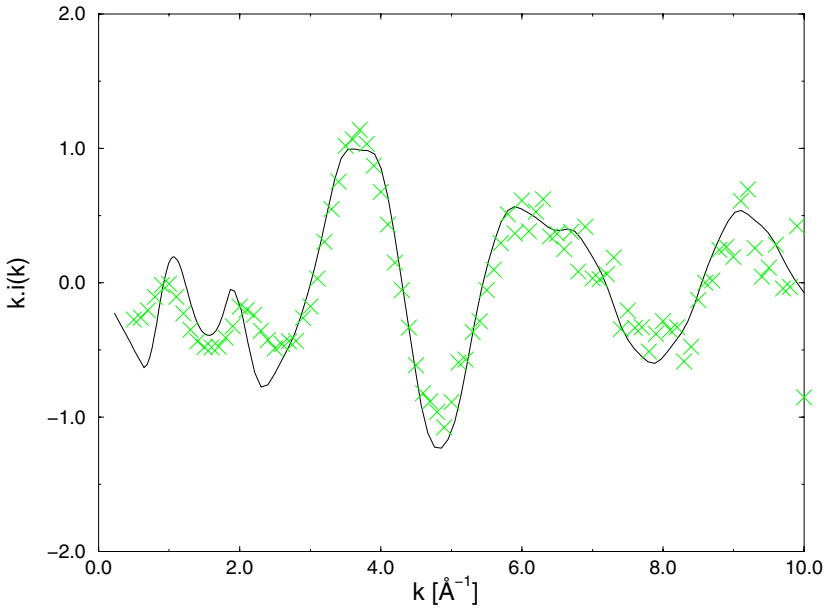

(a)

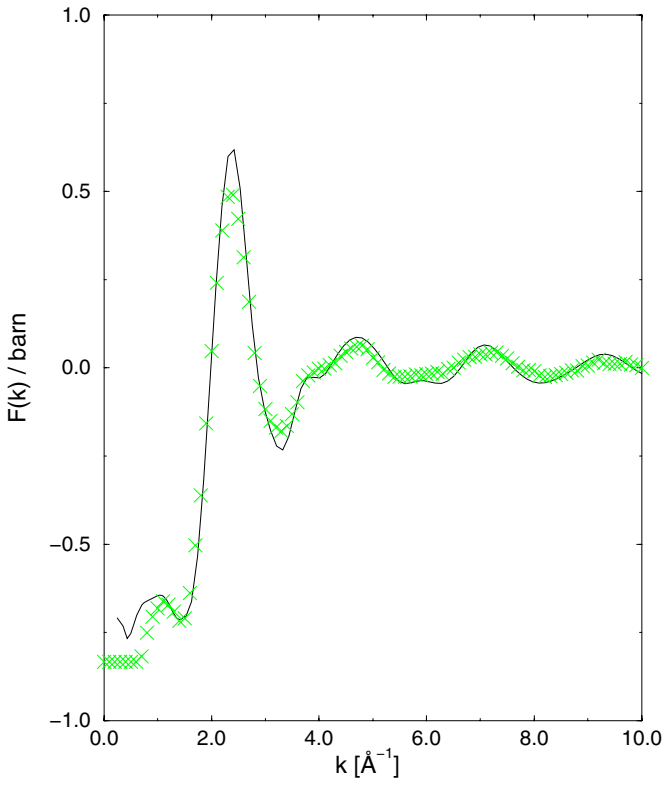

(b)

Figure 7. The comparison between experiment (×) and simulation (lines) for the total neutron structure factor for $LaCl_3$ [23] and the x-ray structure factor (shown $\times k$) for $FeCl_3$ [24], representing the extremes of small and large cations in the MCl_3 family.

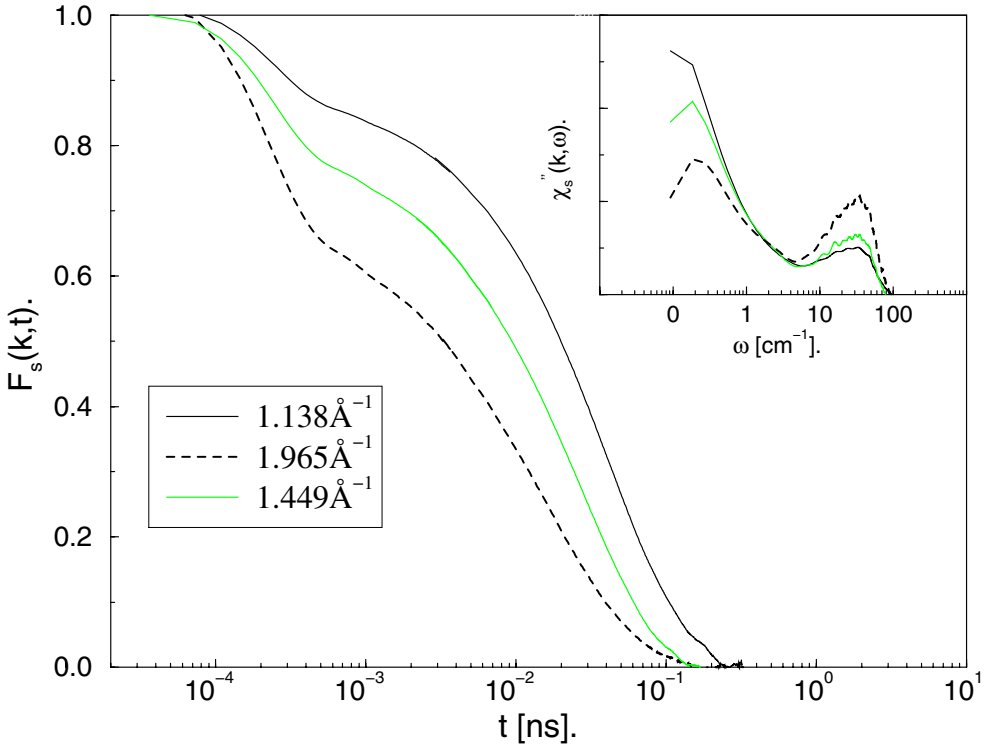

Figure 8. The cation density–density correlation function for $ZnCl_2$ at 700 K at wavevectors corresponding to the positions of the principal peak (≃1.97 Å) of the structure factor (figure 6), the FSDP (≃1.14 Å) and an intermediate position. Inset is the susceptibility of the correlator at the FSDP.

factor reflects *inter*-chain correlations, and its position gives the length scale associated with slow structural relaxation, whereas the principal peak arises from *intra*-chain correlation [30].

4.2. Dynamics on shorter timescales

Spectra of the time correlation functions of figure 8 are shown, in the susceptibility representation, in the inset to that figure. The low-frequency α-peak corresponds to the long-time structural relaxation discussed above. The spectrum above the susceptibility minimum is of similar shape for the liquid and glass and might (crudely) be associated with the oscillations of the ions around some metastable reference configuration which is not changing on the timescale of interest. The optimum description of these oscillations is a matter of active controversy.

The low-frequency oscillations of a simple elastic continuum are the plane-wave acoustic modes of Debye theory. However, when the wavelength of such sound-like excitations approaches the length scale of the intermediate-range order in network systems, they should be strongly scattered by the inhomogeneities which are associated with the IRO (like the voids visible in the snapshots in figures 4) [31, 32]. It has been suggested that this effect is responsible for the excess intensity in the low-frequency density of vibrational states of amorphous systems (relative to expectations from the Debye picture) which is known as the boson peak in spectroscopic studies. The spectra of density fluctuations with wavevectors in the range of interest have recently become available through the development of high-resolution

inelastic x-ray facilities. These spectra show Brillouin-like features [33] (peaks at shifts proportional to k and with widths close to k^2) even for $k \sim k_{FSDP}$. Simulated spectra for $ZnCl_2$ are shown in figure 9, and indicate the same behaviour [34]. Such observations are taken to indicate the persistence of propagating longitudinal acoustic modes to very short wavelengths. The corresponding Brillouin peak frequencies are higher than the boson peak frequency. Examination of the harmonic normal modes in computer simulations shows that the actual modes are more complex than the simple interpretation of the Brillouin peaks would indicate. Individual modes are found to consist of mixtures of plane-wave-like excitations with several wavevectors and polarizations, and these are hybridized with local excitations associated with imperfections in the network. In $ZnCl_2$, for example, the latter involve torsional motions of *edge*-sharing clusters of tetrahedra (recall that the dominant motif involves corner sharing). Whether spectroscopic observations on the low-frequency part of the vibrational region can be satisfactorily explained in terms of the properties of such modes remains to be seen.

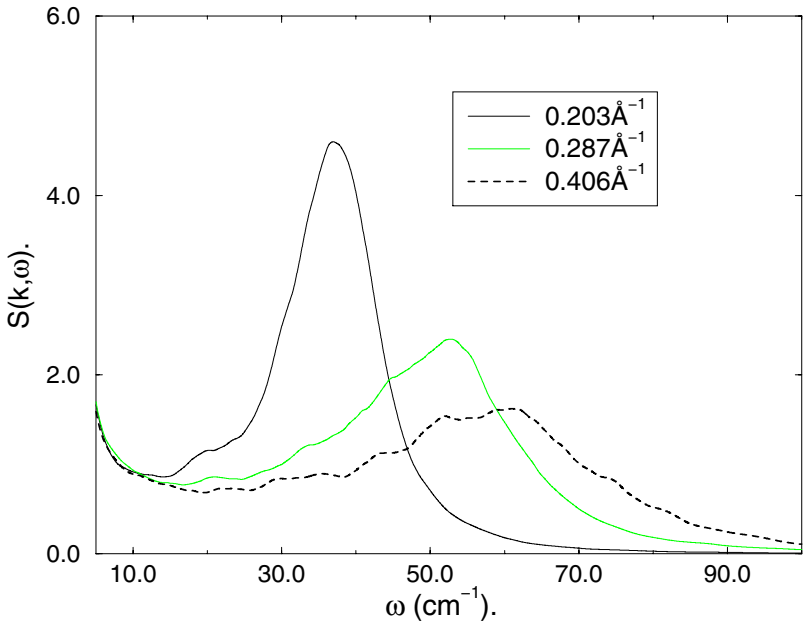

Figure 9. The dynamic structure factor of the mass density of $ZnCl_2$ at 700 K at wavevectors of 0.203, 0.287 and 0.406 Å^{-1}, showing the appearance of Brillouin peaks at large wavevector and frequency.

At still higher frequencies ($>100\,cm^{-1}$), spectroscopic studies of network-forming liquids show broad bands which are interpreted as vibrations of the polyhedral units of which the network is comprised. Controversy persists as to the extent to which the vibrations involving these units can be discussed as if they were the vibrations of isolated molecules. If the network liquid is mixed with a 'structure-breaking' salt, typically containing the same anion, but with a much more weakly coordinating cation (e.g. if CsCl is added to $ZnCl_2$) the network breaks down and individual polynuclear ions form (e.g. $ZnCl_4^{2-}$). In this case, the molecular description seems well justified, but in the undiluted network these units are joined together and the vibrational modes should be more complex. In some cases, it is observed that the spectroscopic structure of the network is very similar to that of the network-broken mixture: in

other cases, bands shift, new bands appear, and band positions appear different in different types of spectroscopy (Raman versus inelastic neutron etc) [35, 36]. To achieve an understanding of the true nature of the vibrational modes in these systems, and an interpretation of the spectroscopic features are important goals. Often, because of the difficulties of making direct structural observations on these liquids, due to the high melting temperature or their corrosive nature, vibrational spectroscopy is the only way of obtaining microstructural information.

References

[1] Rovere M and Tosi M P 1986 *Rep. Prog. Phys* **49** 1001
[2] Tosi M P, Price D L and Saboungi M-L 1993 *Annu. Rev. Phys. Chem.* **44** 173
[3] Woodcock L V and Singer K 1971 *Trans. Faraday Soc.* **67** 12
[4] Biggin S and Enderby J E 1981 *J. Phys. C: Solid State Phys.* **14** 3129
[5] Enderby J E and Barnes A C 1990 *Rep. Prog. Phys.* **53** 85
[6] Stone A J 1996 *Theory of Intermolecular Forces* (Oxford: Clarendon)
[7] Jemmer P, Fowler P W, Wilson M and Madden P A 1998 *J. Phys. Chem.* B **102** 8377
[8] Wilson M, Madden P A, Pyper N C and Harding J H 1996 *J. Chem. Phys.* **104** 8068
[9] Rowley A J, Jemmer P, Wilson M and Madden P A 1998 *J. Chem. Phys.* **108** 10 209
[10] Jemmer P, Wilson M, Madden P A and Fowler P W 1999 *J. Chem. Phys.* **111** 2038
[11] Buckingham A D 1967 *Adv. Chem. Phys.* **12** 107
[12] Madden P A and Wilson M 1996 *Chem. Soc. Rev.* **25** 339
[13] Wilson N T and Madden P A 2000 to be published
[14] Wilson M and Madden P A 1993 *J. Phys.: Condens. Matter* **5** 6833
[15] Brookes R 1998 *Part II Thesis* University of Oxford
[16] Wilson M and Madden P A 1997 *Mol. Phys.* **92** 197
Wilson M and Ribeiro M C C 1999 *Mol. Phys.* **96** 867
[17] Thorpe M F 1983 *J. Non-Cryst. Solids* **57** 533
[18] Phillips J C 1981 *J. Non-Cryst. Solids* **43** 37
[19] Angell C A 1988 *J. Phys. Chem. Solids* **49** 863
Richert R and Angell C A 1998 *J. Chem. Phys.* **108** 9010
[20] Salmon P S 1992 *Proc. R. Soc.* A **437** 591
Salmon P S 1994 *Proc. R. Soc.* A **445** 351
[21] Lee J H and Elliott S R 1995 *J. Non-Cryst. Solids* **193** 133
Ulherr A and Elliott S R 1995 *J. Non-Cryst. Solids* **193** 98
[22] Wilson M and Madden P A 1998 *Phys. Rev. Lett.* **80** 532
Wilson M and Madden P A 1994 *Phys. Rev. Lett.* **72** 3033
[23] Wasse J C and Salmon P S 1998 *Physica* B **241–243** 967
Wasse J C and Salmon P S 1999 *J. Phys.: Condens. Matter* **11** 1381
[24] Badyal Y S, Saboungi M-L, Price D L, Haeffner D R and Shastri S D 1997 *Europhys. Lett.* **39** 19
[25] Hutchinson F *et al* 1999 *J. Chem. Phys.* **110** 5821
Hutchinson F *et al* 1999 *J. Chem. Phys.* **111** 2028
[26] Götze W 1992 *Rep. Prog. Phys.* **55** 341
[27] Kob W and Sciortino F 1999 private communication
[28] Fabbian L *et al* 1998 *Phys. Rev.* E **58** 7272
[29] Wilson M and Madden P A 1994 *J. Phys.: Condens. Matter* **6** A151
[30] Richter D *et al* 1999 *J. Phys.: Condens. Matter* **11** A297
Richter D *et al* 1999 *J. Phys.: Condens. Matter* **11** A363
[31] Elliott S R 1992 *Europhys. Lett.* **19** 201
[32] Orbach R 1996 *Physica* B **220** 231
[33] Sette F *et al* 1998 *Science* **280** 1550
[34] Ribeiro M C C, Wilson M and Madden P A 1998 *J. Chem. Phys.* **108** 9027
[35] Dracopoulos V, Gilbert B and Papatheodorou G N 1998 *J. Chem. Soc. Faraday Trans.* **94** 2601
Zissi G D and Papatheodorou G N 1999 *Chem. Phys. Lett.* **308** 51
[36] Pavlatou E A, Madden P A and Wilson M 1997 *J. Chem. Phys.* **107** 10 446